第 28 卷第 2 期 无 机 化 学 学 报 Vol.28 No.2
2012 年 2 月 CHINESE JOURNAL OF INORGANIC CHEMISTRY 417-424

花状 ZnO/ZnS 异质结构的简易合成、结构表征及光催化活性

李本侠* 王艳芬 吴玉雷
(安徽理工大学材料科学与工程学院,淮南 232001)

摘要: 采用简便的两步溶液相化学方法,在较低温度下(80 ℃),制备出了花状的 ZnO/ZnS 异质结构。分别利用 X 射线衍射、X 射线光电子能谱仪、扫描电子显微镜、透射电子显微镜、紫外-可见光谱仪等测试手段对所制备的样品进行表征,结果表明 ZnO/ZnS 异质结构是由花状 ZnO 纳米结构和 ZnS 纳米粒子组成。在光降解罗丹明 B(RhB)的测试中,ZnO/ZnS 异质结构样品体现出了比 ZnO 前驱物和商业 P25 光催化剂更高的光催化效率,这主要可归因于异质结构更有利于电子-空穴的有效分离。ZnO/ZnS 光催化剂体现出良好的循环稳定性。

关键词: ZnO/ZnS 异质结构; 化学合成; 微结构; 光催化
中图分类号: O649 **文献标识码**: A **文章编号**: 1001-4861(2012)02-0417-08

Flower-Like ZnO/ZnS Heterostructures: Facile Synthesis, Structural Characterization and Photocatalytic Activity

LI Ben-Xia* WANG Yan-Fen WU Yu-Lei
(*School of Science and Engineering of Materials, Anhui University of Science & Technology, Huainan, Anhui* 232001, *China*)

Abstract: ZnO/ZnS heterostructures with flower-like morphology have been prepared via a simple two-step chemical solution method at low temperature (80 ℃). The as-prepared samples were characterized by X-ray diffraction, X-ray photoelectron spectroscopy, scanning electron microscopy, transmission electron microscopy and UV-Vis spectroscopy. The results demonstrate that the ZnO/ZnS heterostructure is composed of ZnO microflower coated by ZnS nanoparticles. In the test for photodegradation of Rhodamine B (RhB), the ZnO/ZnS sample shows higher photocatalytic efficiency than those of ZnO precursor and commercial photocatalyst of P25, which is mainly attributed to the effective electron-hole separation at the interfaces of the heterostructures. The ZnO/ZnS photocatalyst also retains good cycling stability during the photocatalytic degradation of RhB.

Key words: ZnO/ZnS heterostructure; chemical synthesis; microstructure; photocatalysis

The search for highly active photocatalysts for environmental remediation especially waste water decontamination has been a challenging yet very important research topic due to the growing environmental concerns. Photocatalytic degradation of organic pollutants using nanostructured semiconductors offers great potential for the elimination of toxic chemicals[1-3]. ZnO is a wide band-gap semiconductor (3.37 eV) with a conduction band edge located at approximately the same level as that of TiO_2 which has been intensely investigated as a photocatalyst for degradation of organic pollutants. More attractively, the electron mobility of ZnO has been proven to be higher than that of TiO_2[4]. However, despite its great potential, the photocatalytic efficiency remains very low because of the fast recombination of the photogenerated

收稿日期:2011-06-18。收修改稿日期:2011-09-02。
国家自然科学基金(No.21001003),安徽高校省级自然科学研究重点项目(No.KJ2010A101),安徽省自然科学基金(No.10040606Q15)资助项目。
*通讯联系人。E-mail:bxli@aust.edu.cn,Tel:+86-554-6668649,Fax:+86-554-6668643

electron-hole pairs in the single phase semiconductor[5]. Therefore, suppression of the recombination of photogenerated electron-hole pairs in the semiconductors is essential for improving the photocatalytic efficiency. Coupled semiconductors provide routes for promoting the charge separation in semiconductor photocatalysts[6-8]. Integration of two or more desirable semiconductors based on the electron transfer process[9-11], where photogenerated electrons can flow from one semiconductor with a higher conduction band minimum (CBM) to the other with a lower CBM, is of great importance in better realizing photocatalytic degradation of organic pollutants. Compared to single-phase photocatalysts, the coupled semiconductor systems possess significant advantages for promoting the separation of electron-hole pairs and keeping reduction and oxidation reactions at two different reaction sites. Many successful examples have been developed in recent years, such as the semiconductor pairs of SnO_2/ZnO[12], Cu_2O/TiO_2[13], ZnO/In_2O_3[14], ZnO/CeO_2[15], and so on.

The studies in recent years have revealed that ZnS nanocrystals are also good photocatalysts due to the rapid generation of electron-hole pairs by photoexcitation and the highly negative reduction potentials of excited electrons[16-17]. ZnS nanomaterials have been intensively used for photocatalytic degradation of organic pollutants[18] and photocatalytic splitting water for producing H_2[19]. The band structures of ZnS and ZnO are adequate to promote the electron transfer process where photogenerated electrons can flow from ZnS to ZnO[20], and the charge carriers become physically separated upon generation and therefore the recombination rate greatly decreases. Moreover, the theoretical calculations and experimental results have demonstrated that the combination of the two wide bandgap semiconductors of ZnS and ZnO can yield a novel composite with the photoexcitation threshold energy lower than the individual components [21]. Therefore, we selected the ZnO/ZnS system as a target material to synthesize heterostructured nanostructures for photocatalytic degradation of organic pollutant.

Currently, the as-reported heterostructures were mainly concentrated on the biaxial ZnO/ZnS nanowires or nanorods[22-24], whereas the facile synthesis of ZnO/ZnS heterostructures with complex morphology has been rarely reported. Recently, we have synthesized very uniform flower-like ZnO on a large scale through the reaction between Zn^{2+} ions and NaOH in a template- and surfactant-free low-temperature (80 ℃) aqueous solution[25]. Since flower-like ZnO possesses high surface area and open porous surface, they might be ideal platforms to fabricate ZnO/ZnS heterostructures with complex morphology. In this work, ZnO/ZnS heterostructure with a hierarchical 3D flower-like morphology is fabricated by a two-step chemical solution method for use in photocatalytic degradation of organic pollutant. The flower-like ZnO assembled by many interleaving nanosheets were firstly prepared by a simple precipitation, and then sulfuretted partly by an ion exchange process to form ZnS nanoparticles on the ZnO nanosheets. Compared to the ZnO precursor, the as-obtained ZnO/ZnS heterostructure showed an enhanced photocatalytic activity in the photodegradation of rhodamine B.

1 Experimental

1.1 Synthesis of ZnO precursor and ZnO/ZnS heterostructures

All reagents were of analytical grade, purchased from Shanghai Sinopharm Chemical Reagent Co. Ltd. and used without further purification.

Firstly, the flower-like ZnO was prepared through a simple precipitation method by reacting $ZnCl_2$ and NaOH in aqueous solution, similar to that described in our previous paper[25]. 2.0 mmol $ZnCl_2$ and 10.0 mmol NaOH were dissolved in 30 mL of distilled water under stirring, and the mixed solution was sealed in a glass bottle (60 mL), kept static at 80 ℃ for 12 h. The final white precipitate was separated by centrifuge, washed with distilled water and absolute alcohol several times to remove the possible residues, and then dried in air.

An ion-exchange process was adopted to prepare the ZnO/ZnS heterostructures. The as-prepared ZnO precursor was dispersed in aqueous solution of Na_2S (0.05 mol·L^{-1}) and heated in an oven at 80 ℃ for 8 h.

The resultant product was then rinsed with distilled water, and dried for further characterization.

1.2 Characterizeation of ZnO precursor and ZnO/ZnS heterostructures

The XRD patterns were recorded on a Japan Rigaku D/max-rA X-ray diffractometer equipped with a graphite diffracted-beam monochromator for Cu $K\alpha$ radiation (λ =0.154 178 nm) at 40 kV and 200 mA, using 0.15 mm receiving slit and scintillation counter as the detector. The 2θ region was in the range of 10°~ 70° with a step of 0.02° and a scanning speed of 4°·min^{-1}. The field emission scanning electron microscopy (FESEM) was performed on JEOL JSM-6700F at an accelerating voltage of 20 kV, and transmission electron microscopy (TEM) images associated with energy-dispersive X-ray spectroscopy (EDS) were performed on JEOL-2010 TEM with an acceleration voltage of 200 kV. X-ray photoelectron spectroscopy (XPS) provided further evidences for the component of ZnO/ZnS heterostructure, and the measurements were performed on a VGESCALAB MKII X-ray photoelectron spectrometer with an excitation source of Mg $K\alpha$ = 1253.6 eV. The binding energies in the XPS analysis were corrected for specimen charging by referencing the C1*s* to 284.60 eV. The UV-Vis diffuse reflectance spectra (DRS) were recorded on a DUV-3700 DUVVISNIR recording spectrophotometer from Shimadzu Corporation.

1.3 Photocatalytic activity test

The photocatalytic performance of the as-prepared products was evaluated by decomposing the model pollutant of Rhodmine B (RhB) under UV irradiation from a 200-W high-pressure Hg lamp (the strongest emission at 365 nm) at room temperature. The distance between the light source and the solution surface was set at about 10 cm. In the degradation experiment, 50 mg of photocatalyst was suspended in 100 mL of a 5.0×10^{-5} mol·L^{-1} aqueous solution of RhB. Prior to irradiation, the suspensions were stirred in dark for 1 h to establish an adsorption/desorption equilibrium. At time intervals, about 5 mL of the solution was taken from the reaction beaker for analysis of the RhB concentration after centrifuging. The photocatalytic degradation process was monitored by measuring the absorption of RhB at 553 nm on a UV-Vis spectrop hotometer (Shimadzu UV2550).

2 Results and discussion

2.1 XRD, SEM, TEM and XPS characterization

In this work, ZnO/ZnS heterostructure was fabricated by a two-step chemical solution method. After the flower-like ZnO precursor was obtained[25], it was used to fabricate ZnO/ZnS heterostructured microflowers by ion exchange between ZnO precursor and S^{2-}, as described in Scheme 1. Compared with the usual coprecipitation, this strategy can avoid the quick nucleation and growth of ZnS in the solution, and ZnS nanoparticles in situ formed on the surface of ZnO to form ZnO/ZnS heterostructure.

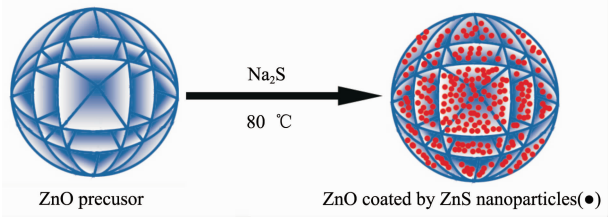

Scheme 1　Scheme for the preparation of ZnO/ZnS heterostructure.

Fig.1 displays XRD patterns of the ZnO precursor and ZnO/ZnS heterostructure. In the XRD pattern of ZnO precursor (Fig.1a), all the diffraction peaks can be accurately assigned to hexagonal wurtzite ZnO (PDF No. 36-1451). The XRD pattern of the ZnO/ZnS heterostructure (Fig.1b) indicates that there are two sets of patterns: one can be assigned to hexagonal wurtzite

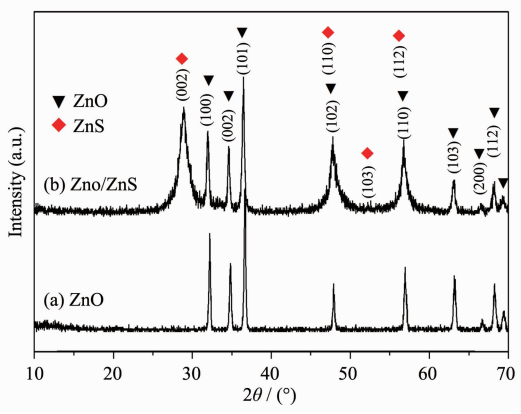

(a) ZnO precursor; (b) ZnO/ZnS heterostructure

Fig.1　XRD patterns of the as-prepared samples

ZnO and the other originates from hexagonal wurtzite ZnS (PDF No. 80-0007). The diffraction peaks of ZnO are sharp and intense, revealing the highly crystalline character of the ZnO component, while the diffraction peaks of ZnS are broad and weak, indicating a small crystal size or semicrystalline nature of the ZnS component[26].

Fig.2a~b show SEM images of the ZnO precursor, revealing that the morphology of ZnO product is well-defined flower-like three-dimension (3D) microstructures with diameters in the range of 1~2 μm, assembled by nanosheets as "petals". A close-up view in Fig.2b shows that the nanosheets are about 10 nm in thickness, and they alternately connect with each other to form a network-like surface of the "flower". Many pores with different sizes are engendered in the 3D microflowers, which may improve the chemical properties or serve as transport paths for small molecules.

Fig.2c~d show SEM images of ZnO/ZnS heterostructures prepared by the ion exchange for 8 h. It is found that the morphology of ZnO/ZnS heterostructures still present 3D flower-like hierarchical structures, suggesting that the ion-exchange process does not damage the flower-like morphology of ZnO precursor. Besides, there are many nanoparticles with the sizes of several nanometers growing on the surfaces of the ZnO nanosheets, and the surfaces become coarse compared with those of ZnO precursor. Accordingly, it can be concluded that the as-prepared ZnO/ZnS heterostructural microflowers are composed of flower-like ZnO coated by ZnS nanoparticles. Importantly, this coarse-surface structure can enhance the dye absorption and diminish the reflection of the incident light [27], which may greatly improve the photocatalytic performance.

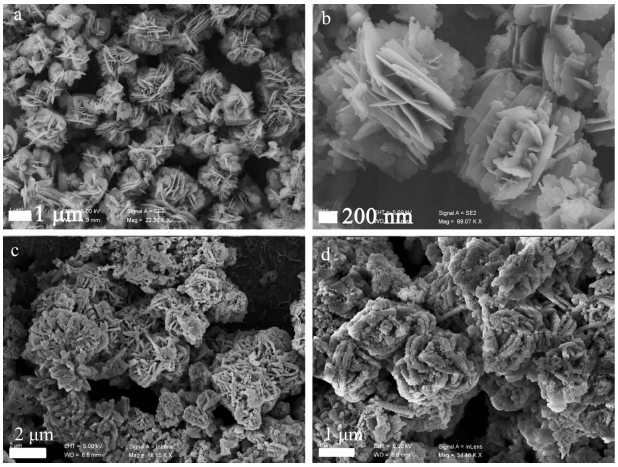

Fig.2 SEM images for (a~b) ZnO precursor, (c~d) ZnS/ZnO heterostructure

The detailed structures and compositions of ZnO/ZnS heterostructure were further investigated using transmission electron microscopy (TEM) and energy-dispersive X-ray spectroscopy (EDS). Fig.3a shows a low-magnification TEM image of ZnO/ZnS heterostructure, indicating ZnS nanoparticles are grown on ZnO nanosheet. Fig.3b, c show the HRTEM images for two representative segments from one of the nanosheets, as marked with frames in Fig.3a, to map out the distribution of crystal structures. The lattice distance in Fig.3b taken from the edge with a light contrast of the nanosheet is 0.261 nm, corresponding to the (0002) plane of wurtzite ZnO. The other lattice distance in Fig.3c taken from the middle part with a dark contrast of the nanosheet is 0.312 nm, corresponding to the (0002) plane of wurtzite ZnS. However, the interface segment of ZnO and ZnS cannot

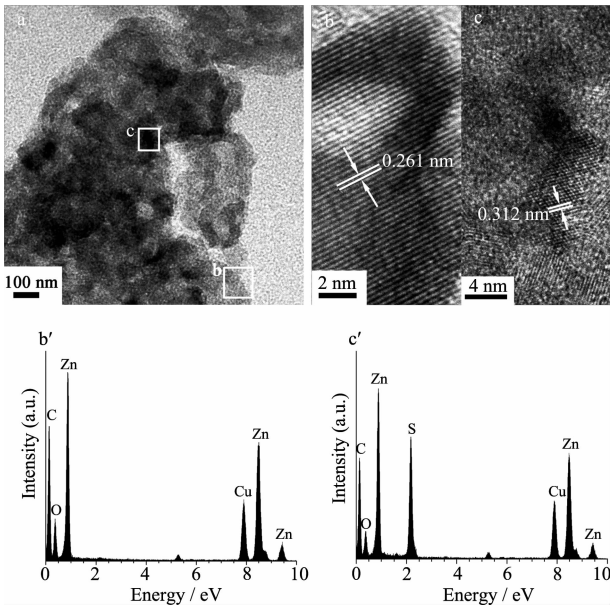

Fig.3 (a) TEM image for a fragmented nanosheet from the ZnO/ZnS heterostructure. (b, c) HRTEM images recorded from the frame marked regions b and c, respectively, in (a); (b′, c′) EDS spectra taken from the frame marked regions b and c, respectively, in (a)

be observed because the overlapping orientation of ZnO nanosheet and ZnS nanoparticles. EDS data were collected from two selected areas marked with frames of b and c in Fig.3a, and the spectra are shown in Fig.3b′ and c′, respectively. The results show that the part with light contrast mainly consists of Zn and O, and the other part with dark contrast is mainly composed of Zn and S. The signals of C and Cu in the EDS spectra originate from the carbon-coated copper grid for TEM measurement. Thus, both TEM and EDS results consistently prove the formation of ZnO/ZnS heterostructure.

The XPS results are shown in Fig.4. The survey spectrum in Fig.4(a) reveals the presence of Zn, S, O elements without any other contaminant species, except for a small amount of carbon. The Zn2*p* core level XPS spectrum in Fig.4(b) is centered at 1 021.8 eV, which is attributed to the Zn2$p_{3/2}$ of Zn^{2+}[12]. Fig.4(c) shows the O1*s* core level peak at 531.2 eV, which agrees well with the O1s of O^{2-}. The binding energies of S2*p* shown in Fig.4(d) for ZnO/ZnS is 161.9 eV, smaller than those of sulfur and related compounds (S^0: 164.0 eV; SO_2: 163-165.5 eV; SO_3^{2-}: 166.4 eV; SO_4^{2-}: 168~170 eV), which is consistent with the reported value for ZnS in ZnO/ZnS heterostructure [28]. Therefore, the XPS spectra confirm that the ZnO/ZnS sample is composed of Zn^{2+}, O^{2-} and S^{2-}.

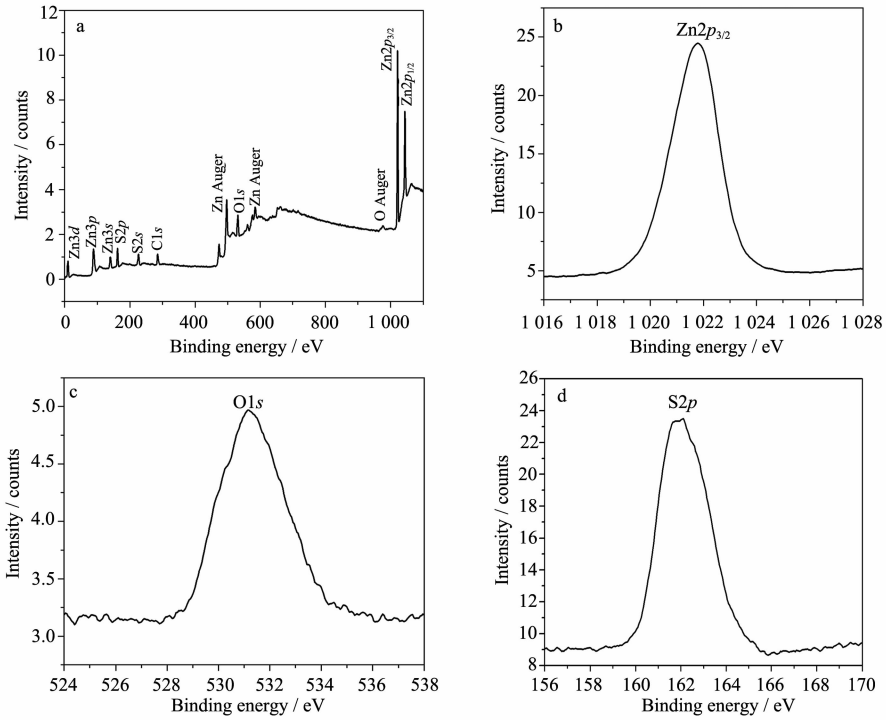

(a) the survey spectrum; (b) Zn2$p_{3/2}$; (c) O1s; (d) S2*p*

Fig.4　XPS spectra for ZnO/ZnS heterostructures

2.2　UV-Vis diffuse reflectance spectrum

Fig.5 shows UV-Vis diffuse reflectance spectra for ZnO precursor and ZnO/ZnS heterostructure, which reveals the remarkable change of the optical absorption property of the sample after combining another semiconductor. In Fig.5a, ZnO precursor exhibits a strong absorption in ultraviolet region with spectral wavelength between 200 and 400 nm. The energy of the band gap of the direct band-gap semiconductor could be estimated from the plots of $(\alpha h\nu)^2$ versus photon energy ($h\nu$), and the estimated band-gap of ZnO precursor is 3.24 eV, shown in the inset of Fig.5a. In the UV-Vis absorption spectrum of ZnO/ZnS heterostructure (Fig.5b), there are two absorption edges which can be assigned to the characteristic absorption of ZnS and ZnO components, respectively. The appearance of two kinds of characteristic absorption edges also confirms that the ZnO/ZnS sample is a

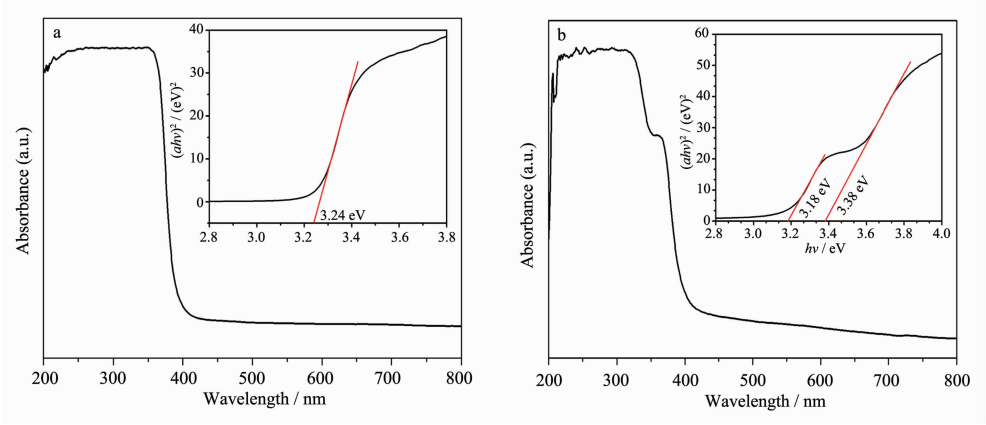

(a) ZnO precursor, (b) ZnO/ZnS heterostructures
Inset is the band gaps/E_g estimated from the absorption edge

Fig.5 UV-Vis diffuse reflectance spectra for the samples

composite semiconductor composed of ZnO and ZnS. The estimated band-gaps of ZnO and ZnS component in ZnO/ZnS heterostructure are 3.18 eV and 3.38 eV, respectively, smaller than the reported values of ZnO (3.23 eV)[25] and ZnS (3.7 eV)[20], which may result from the interfacial combination and matched band edges between the two semiconductors of ZnO and ZnS.

2.3 Photocatalytic degradation of Rhodamine B (RhB)

Fig.6 (a) shows the UV-Vis absorption spectrum of RhB aqueous solution (initial concentration: 5.0×10^{-5} mol·L^{-1}, 100 mL) with 50 mg of ZnO/ZnS

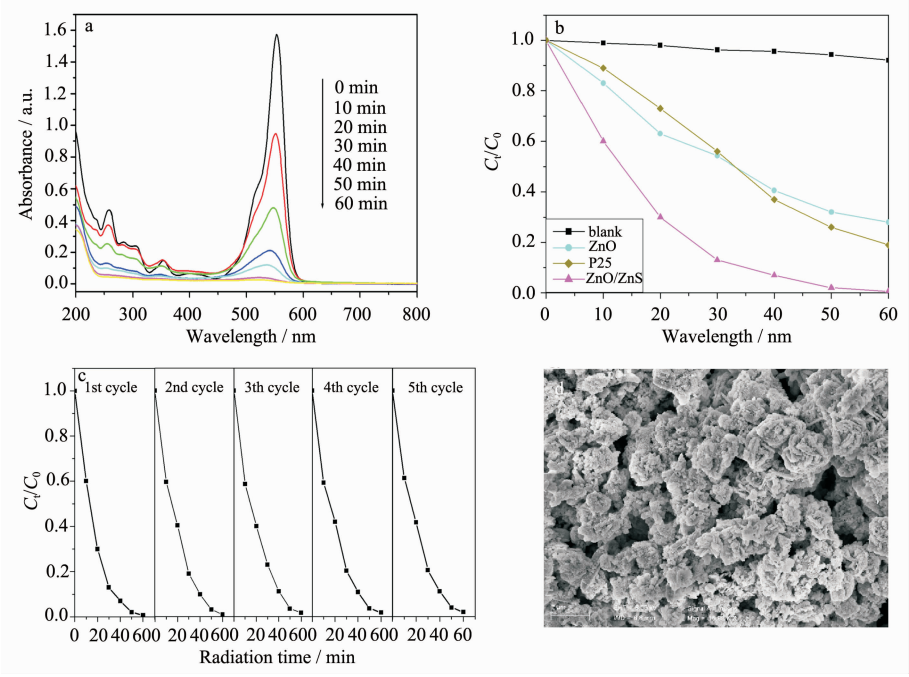

Fig.6 (a) UV-Vis absorption spectra for the RhB solution (5×10^{-5} mol·L^{-1}, 100 mL) in the presence of 50 mg of ZnO/ZnS heterostructures under UV light irradiation. (b) Photodegradation of RhB (5×10^{-5} mol·L^{-1}, 100 mL) using different photocatalysts under UV light irradiation. (c) The variation of the concentration of RhB solution versus illumination time with ZnO/ZnS heterostructures as photocatalyst under UV light irradiation during the five cycles. (d) SEM image for the recycled ZnO/ZnS photocatalyst after five cycles

heterostructures as photocatalyst and exposure to the irradiation for various durations. The characteristic absorption of RhB at 553 nm decreases rapidly with extension of the exposure time, and completely disappears after about 60 min. Fig.6 (b) shows the results of the RhB degradation under different conditions, where C_0 and C_t are the initial concentration after the equilibrium adsorption and the reaction concentration of RhB, respectively. A blank test (RhB without any catalyst) under irradiation exhibits little decrease in the concentration of RhB. For the pure ZnO (ZnO precursor), the RhB degradation is about 70% after 60 min. For ZnO/ZnS heterostructures, the photodegradation of RhB reaches nearly 100% after 60 min. Moreover, ZnO/ZnS heterostructures show higher photocatalytic efficiency than that of the well-known photocatalyst of P25 TiO_2 (purchased from Degussa). Because the stability of a photocatalyst is important and necessary for its application, five cycles of the photocatalytic experiment for the ZnO/ZnS heterostructures were carried out to investigate the repeatability of the photocatalyst. As shown in Fig.6c, RhB could be totally decomposed in each cycle and the ZnO/ZnS photocatalyst exhibits almost no change in its photocatalytic activity during the repeated photocatalytic experiments. Fig.6d shows a SEM image of the recycled ZnO/ZnS photocatalyst after five cycles, and it indicates that the morphology of the photocatalyst almost remains unchanged. Thus, the enhanced photocatalytic activity and stable capacity retention of ZnO/ZnS heterostructures are beneficial for the potential application as a photocatalyst.

The factors inducing the enhanced photocatalytic activity of the ZnO/ZnS heterostructures are complicated. However, the electron-hole separation at the ZnO/ZnS interfaces must be a critical one. On the basis of the Anderson model[29], a "staggered" type II band configuration at the interface of the ZnO/ZnS heterostructure is proposed, as shown in Fig.7. Due to both ZnO and ZnS have adsorption response to the UV irradiation, electrons (e^-) in the valence bands (VB) are excited to their conduction bands (CB), with the same amount of holes (h^+) left in VB. The interfacial electron-

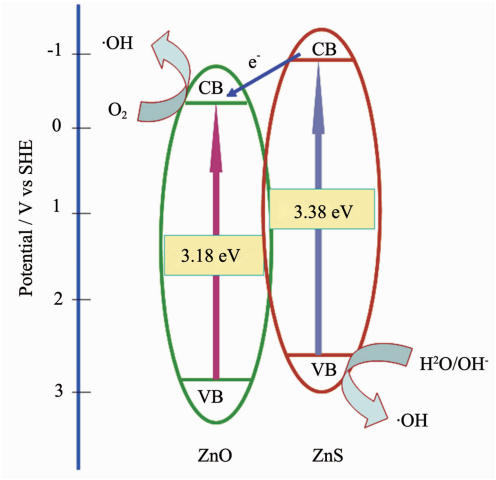

Fig.7　Schematic diagram showing band configuration and electron-hole separation at interface of ZnO/ZnS heterostructure under UV light

hole separation in ZnO/ZnS heterostructures would be bidirectional. The photogenerated electrons in CB of ZnS incline to transfer to CB of ZnO with a lower potential, while the holes in VB of ZnO transfer to VB of ZnS with a higher potential [27]. Consequently, the photogenerated electrons and holes are separated at the ZnO/ZnS interfaces, which suppresses their recombination probability and enables them to migrate effectively to the surfaces of ZnO and ZnS, respectively, to form the hydroxyl radicals (·OH)[30]. As a powerful oxidant, the hydroxyl radicals could decompose effectively the organic pollution, and thus the photocatalytic reaction can be enhanced greatly.

3　Conclusions

ZnO/ZnS hetero structures with a hierarchical morphology were fabricated by a facile two-step chemical solution method for use in photocatalytic degradation of organic pollutant. The ZnO/ZnS heterostructures are composed of ZnO microflowers coated by ZnS nanoparticles. As a photocatalyst for photodegradation of RhB, the ZnO/ZnS sample shows higher photocatalytic efficiency than those of the ZnO precursor and P25 TiO_2, which is mainly attributed to the effective electron-hole separation at the interfaces of the heterostructures. Moreover, the ZnO/ZnS photocatalyst also retains good cycling stability during the photocatalytic degradation of RhB.

References:

[1] Albu S P, Ghicov A, Macak J M, et al. *Nano Lett*., **2007**,**7**: 1286-1289

[2] Yang D J, Liu H W, Zheng Z F, et al. *J. Am. Chem. Soc*., **2009**,**131**:17885-17893

[3] Wu N Q, Wang J, Tafen D N, et al. *J. Am. Chem. Soc*., **2010**, **132**:6679-6685

[4] Keis K, Bauer C, Boschloo G, et al. *J. Photochem. Photobiol. A*: *Chem*., **2002**,**148**:57-64

[5] Hoffmann M R, Martin S T, Choi W, et al. *Chem. Rev*., **1995**, **95**:69-96

[6] YANG Juan(杨娟), LI Jian-Tong(李建通), MIAO Juan(缪娟). *Chinese J. Inorg. Chem*. (*Wuji Huaxue Xuebao*), **2011**,**27**: 547-555

[7] Colón G, López S M, Hidalgo M C, et al. *Chem. Commun*., **2010**,**46**:4809-4811

[8] Li B X, Wang Y F. *Superlatt. Microstr*., **2010**,**47**:615-623

[9] Shang M, Wang W Z, Zhang L, et al. *J. Phys. Chem. C*, **2009**,**113**:14727-14731

[10]Peng L L, Xie T F, Lu Y C, et al. *Phys. Chem. Chem. Phys*., **2010**,**12**:8033-8041

[11]Wang X W, Liu G, Chen Z G, et al. *Chem. Commun*., **2009**, **23**:3452-3454

[12]Zheng L R, Zheng Y H, Chen C Q, et al. *Inorg. Chem*., **2009**,**48**:1819-1825

[13]Lalitha K, Sadanandam G, Kumari V D, et al. *J. Phys. Chem. C*, **2010**,**114**:22181-22189

[14]Wang Z Y, Huang B B, Dai Y, et al. *J. Phys. Chem. C*, **2009**,**113**:4612-4617

[15]Ma T Y, Yuan Z Y, Cao J L. *Eur. J. Inorg. Chem*., **2010**,**5**: 716-724

[16]Hu J S, Ren L L, Guo Y G, et al. *Angew. Chem. Int. Ed*., **2005**,**44**:1269-1273

[17]WU Xiao(吴晓), WANG Hao(汪浩). *Chinese J. Inorg. Chem*. (*Wuji Huaxue Xuebao*), **2010**,**26**:453-458

[18]Chen D G, Huang F, Ren G Q, et al. *Nanoscale*, **2010**,**2**: 2062-2064

[19]Tsuji I, Kato H, Kobayyashi H, et al. *J. Am. Chem. Soc*., **2004**,**126**:13406-13413

[20]Schrier J, Demchenko D O, Wang L W. *Nano Lett*., **2007**,**7**: 2377-2382

[21]Lahiri J, Batzill M. *J. Phys. Chem. C*, **2008**,**112**:4304-4307

[22]Murphy M W, Grace Kim P S, Zhou X T, et al. *J. Phys. Chem. C*, **2009**,**113**:4755-4757

[23]Yan J, Fang X, Zhang L, et al. *Nano Lett*., **2008**,**8**:2794-2799

[24]Lin D D, Wu H, Zhang R, et al. *J. Am. Ceram. Soc*., **2010**, **93**:3384-3389

[25]Li B X, Wang Y F. *J. Phys. Chem. C* **2010**,**114**:890-896

[26]Klug H, Alexander L. *X-ray Diffraction Procedure*. New York: Wiley, **1962**.125.

[27]Yu X L, Song J G, Fu Y S, et al. *J. Phys. Chem. C*, **2010**, **114**:2380-2384

[28]Chen P, Gu L, Cao X B. *CrystEngComm*, **2010**,**12**:3950-3958

[29]Anderson R L. *Solid State Electron*., **1962**,**5**:341-351

[30]Gnaser H, Savina R M, Calaway F W, et al. *Int. J. Mass Spectrom*., **2005**,**245**:61-67